The Astrophysical Journal, 975:164 (10pp), 2024 November 10 https://doi.org/10.3847/1538-4357/ad7a6e

Quasiperiodic γ-Ray Modulations in the Blazars PKS 2155-83 and PKS 2255-282

M. A. Hashad[1,2], Amr A. EL-Zant[2], Y. Abdou[3], and H. M. Badran[3]
[1] Department of Basic Science, Modern Academy for Engineering and Technology, Elmokattam 11439, Egypt; Mohamed.Hashad@bue.edu.eg
[2] Centre for Theoretical Physics, The British University in Egypt, Sherouk City, 11837, Cairo, Egypt
[3] Physics Department, Faculty of Science, Tanta University, Tanta, 31527, Gharbia, Egypt
Received 2024 July 9; revised 2024 August 27; accepted 2024 September 10; published 2024 October 31

Abstract

While there has been an increase in interest in the possibility of quasiperiodic oscillations (QPOs) in blazars, the search has hitherto been restricted to sources with well-sampled light curves. Objects with light curves that include gaps have been, to our knowledge, overlooked. Here, we study two such curves, which have the interesting feature of pertaining to relatively high-redshift blazars—FSRQs, PKS 2155-83, and PKS 2255-282—observed by the Fermi Large Area Telescope. Their redshifts border the "cosmic noon" era of galaxy formation and merging, and their light curves exhibit a distinctive pattern of repetitive high and low (gap dominant) states for 15.6 yr. To accommodate for the gaps in the curves, data are integrated over extended time intervals of 1 month and 2 months. The resulting curves were also examined using methods suitable for sparsely sampled data. This investigation of PKS 2155-83 and PKS 2255-282 suggests QPOs with periods of 4.69 ± 0.79 yr (3σ) and 6.82 ± 2.25 yr (2.8σ), respectively. The probability density functions of the blazars' fluxes, along with the correlation between their flux and spectral index, were also analyzed. Given the epochs in which the objects are observed, the plausibility of a binary black hole scenario as an origin of the apparent periodicity was examined. We estimated the prospective parameters of such a system using a simple geometric model. The total masses were estimated and found to be consistent, in principle, with independent (dynamical) measurements of the central black hole masses in the two host galaxies.

Unified Astronomy Thesaurus concepts: Active galactic nuclei (16); Gamma-ray astronomy (628); Time series analysis (1916); Non-thermal radiation sources (1119); Galaxy mergers (608); Blazars (164)

1. Introduction

Collimated plasma jets are launched from active galactic nuclei (AGN) born of spinning black holes (BHs) and strongly magnetized accretion disks. Blazars are a class of AGN whose relativistic jets nearly point to the line of sight connecting it to the Earth, and are dominated by nonthermal emission (C. M. Urry & P. Padovani 1995; G. G. Madejski & M. Sikora 2016; R. Blandford et al. 2019). Owing to the jet's alignment and its narrow opening, Doppler enhancement is expected of the blazar emission and, subsequently, contract the timescales of its variability (D. Yan et al. 2018).

Erratic variability in blazars' emission has been observed over almost all the electromagnetic spectrum and over a wide range of timescales (M. Błazejowski et al. 2005; N. H. Liao et al. 2014; G. Bhatta & N. Dhital 2020; J. Abhir et al. 2021). In particular, virtue of the continuous all-sky monitoring of the Fermi Large Area Telescope (Fermi-LAT; W. B. Atwood et al. 2009), launched in 2008, one can seek out and check for quasiperiodicity in γ-ray blazars with periods up to a few years. Numerous recent results have indeed found evidence for the existence of such quasiperiodic variability in blazars (D. A. Prokhorov & A. Moraghan 2017; A. Sandrinelli et al. 2018; M. Tavani et al. 2018; F. A. Benkhali et al. 2020; P. Peñil et al. 2020; P.-f. Zhang et al. 2020; M. Hashad et al. 2023; H. X. Ren et al. 2023).

After six years of Fermi-LAT data gathering, the first evidence of a significant QPO ($\sim 3\sigma$) in γ-ray light curve (LC) has been reported for PG 1553+113 with a period of 2.18 yr (M. Ackermann et al. 2015). One remarkable case is PKS 2247-131, which manifests a short periodicity ($\sim$34.5 days) in its γ-ray LC from 2016 November to 2017 June with six cycles at high significance (5.2σ; J. Zhou et al. 2018). This QPO has been interpreted in terms of a helical structure in the jet. Using 12 yr of Fermi-LAT data, P. Peñil et al. (2022) have examined the γ-ray LCs of the most promising 24 periodicities reported in the literature. Five blazars with γ-ray QPOs observed with significance $\gtrsim 3\sigma$ have been found, one flat-spectrum radio quasar (FSRQ), PKS 0454-234, and four BL Lac objects, OJ 014, PG 1553+113, S5 0716+714, and PKS 2155-304. Observing such periodic signals could provide insight into blazars' nature and BH–jet systems.

Indeed, the mechanism producing possible γ-ray QPOs in blazars is not entirely understood. Scenarios like jet precession, pulsational accretion flow instabilities, and the existence of binary BH systems have been proposed (e.g., M. Ackermann et al. 2015; E. Sobacchi et al. 2017; A. Caproni et al. 2017). The broadness of the possibilities is reflected in the fact that, within the variety of models of QPOs in blazars, the QPOs can originate from intrinsic as well as apparent origins; in the intrinsic scenario, QPO is assumed to exist in the relativistic jet's comoving frame, while an apparent origin refers to a periodically changing viewing angle and associated Doppler factor, which in turn boosts the observed flux periodically.

The reported searches for quasiperiodicity usually focus on objects with LCs that have significant detections in most bins. Typically, the minimum detection significance of the bins is set to be $\geqslant 3\sigma$. As a result, important attributes in LCs with many upper limits or gaps are generally neglected.

In this work, we introduce the results of a QPO search in two moderate-redshift blazars: FSRQs PKS 2155-83 ($z = 1.865$) and PKS 2255-282 ($z = 0.926$). Both exhibit the distinguishing behavior of repetitive high states and extremely faint epochs. These faint epochs are considered low (quiescent) states where upper limits and gaps frequently exist, particularly for time binning of narrow time intervals. Here, we examine longer binning intervals and use methods that are suitable for time series with gaps, in order to attempt to reveal possible QPO signals. The redshifts, bordering the "cosmic noon" era of galaxy formation and merging (in some definitions, PKS 2155-83 being well within that epoch), may hint at the apparent QPO being suitable candidates to be associated with supermassive black hole (SMBH) merger events (M. C. Begelman et al. 1980; P. Madau & M. Dickinson 2014; S. Komossa et al. 2016; M. Volonteri et al. 2016; Y. Yang et al. 2020; M. Mezcua et al. 2024).

Our search is based on Fermi-LAT data over about 15.6 yr. A detailed analysis of Fermi-LAT data is presented in Section 2. The resulting LCs are then examined for possible quasiperiodicities, using various methods, in Section 3. Section 4 summarizes the results and discusses the findings.

2. Data Analysis

2.1. The Fermi-LAT Light Curves

The Fermi Gamma-ray Space Telescope is a space mission with two scientific instruments: the LAT and the Gamma-ray Burst Monitor. The Fermi-LAT high-energy γ-ray telescope covers the energy range from about 20 MeV up to 1 TeV and owns a large effective area ($\sim$8000 cm^2 at 1 GeV), with $\sim$2.4 sr field of view and a point-spread function of $<0.^\circ 8$ above 1 GeV (W. B. Atwood et al. 2009). LAT scans the whole celestial sphere every 3 hr. The instrument took off on 2008 June 11, and is still in operation. In the course of its 15 yr operation, it detected high-energy γ-rays from assorted classes of objects with the most severe conditions, including but not limited to γ-ray blazars.

We consider here the LCs of two blazars detected by the Fermi observatory, searching within them for quasiperiodic signals. The distant FSRQ PKS 2155-83 is at R.A. $= 330^{\rm h}36^{\rm m}00.^{\rm s}00$ and decl. $= 83^{\rm d}35^{\rm m}60.^{\rm s}0$, J2000 (T. Mauch et al. 2003; C. Fabricius et al. 2021). It was observed by Fermi-LAT in a high state on 2010 January 5, with a γ-ray flux $F(E > 100\ \mathrm{MeV})$ of $(1.4 \pm 0.3) \times 10^{-6}$ photons cm^{-2} s^{-1}, which is more than 1 order of magnitude larger than the average flux during the first 11 months of observations (E. Wallace 2010). According to the Fermi-LAT fourth source catalog (4FGL-DR3; S. Abdollahi et al. 2022), PKS 2155-83 (4FGL J2201.5-8339) has an average detection significance of 41.88σ with a predicted photon number of 4247.39 and flux fractional variability of $67.86 \pm 14.84\%$. During the 15.6 yr of Fermi-LAT observations, the object has had eminent behavior, where it seems to release four high states in 2010, 2014, 2019, and 2023 throughout its low state, as shown in the LCs in Figure 1. This behavior may underline a featured origin, as the repeated high states look periodic.

Similarly, another distant FSRQ, PKS 2255-282—with R.A. $= 344^{\rm h}30^{\rm m}00.^{\rm s}00$ and decl. $= -27^{\rm d}53^{\rm m}60.^{\rm s}0$, J2000 (D. H. Jones et al. 2009)—shows three high states (2009–2013, 2017–2021, and 2023 up to the end of data) throughout its low state, as shown in Figure 2. An average

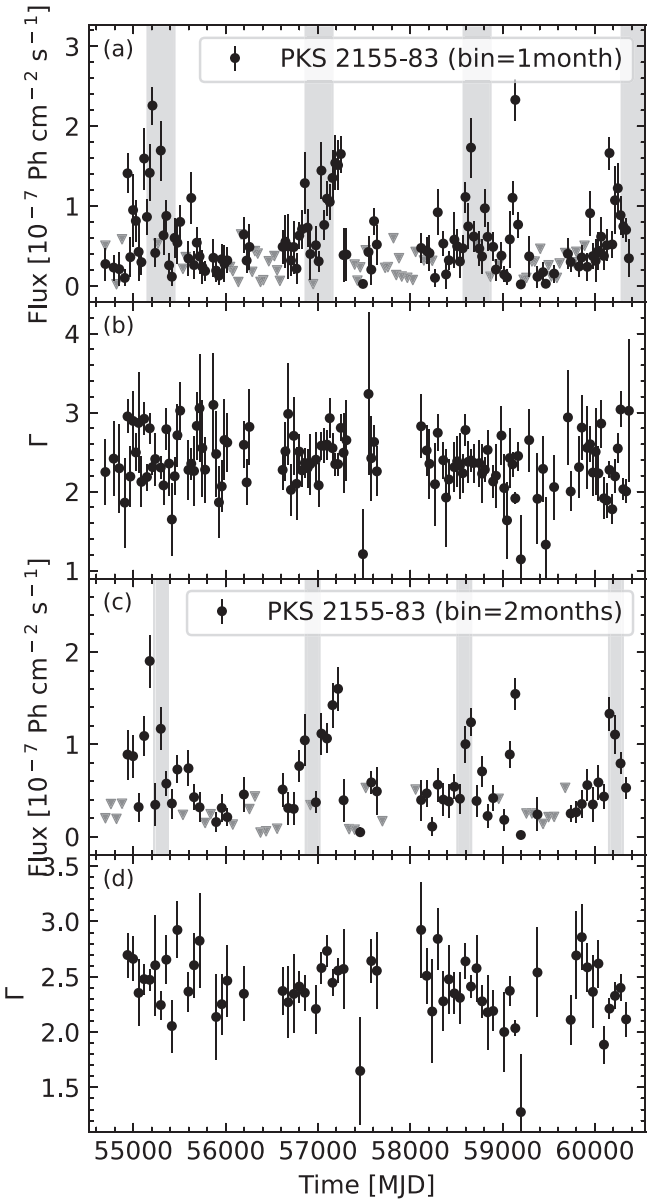

Figure 1. PKS 2155-83 LCs in the energy range from 100 MeV to 500 GeV between 2008 August 4, and 2024 February 29. Showing (a) the 1 month binned LC, (b) the photon spectral index of (a), (c) 2 month binned LC, and (d) the photon spectral index of (c). In panels (a) and (c), filled black points denote significant detections, with $TS > 4$ for the 1 m binned LC and $TS > 9$ for the 2 m binned LC. Downward gray arrows denote 95% confidence level upper limits. The gray vertical columns approximately delineate periods of high states, inferred from the generalized Lomb–Scargle periodogram. The periodic signals' uncertainty is indicated by the width of the gray columns. The photon index is plotted only for the detected bins. In all panels, vertical error bars are 1σ error.

detection significance of 66.57σ, a predicted photon number of 7383.77, and flux fractional variability of $84.67 \pm 18.17\%$ were reported from the source in Fermi's fourth catalog (S. Abdollahi et al. 2022). Radio measurements at 15 GHz (M. L. Lister et al. 2009) and 22 and 43 GHz (P. Charlot et al. 2010) suggested a compact object with a core-dominated structure. The object was in a high state on 2012 February 26, with a γ-ray average daily flux above 100 MeV of $(1.0 \pm 0.3) \times 10^{-6}$ photons cm^{-2} s^{-1}. This exemplifies a boost factor of $\sim$14 above its average flux in Fermi's second catalog (M. Dutka et al. 2012). It was the first significant Fermi-LAT source to be detected at such a high value

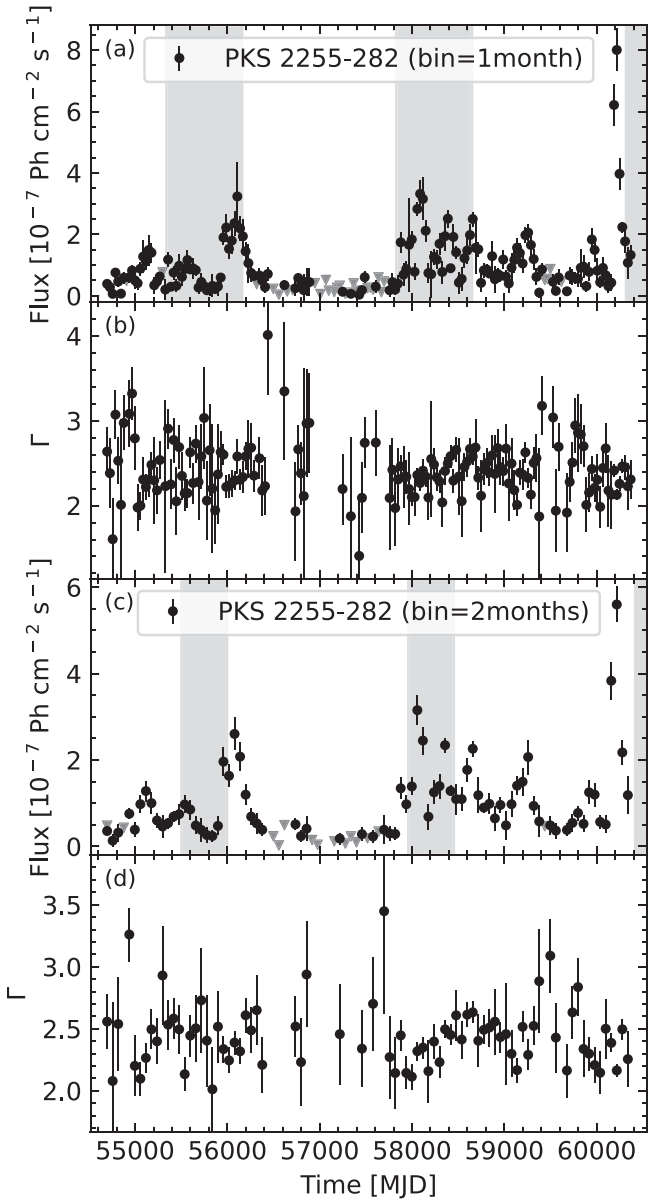

Figure 2. The same as Figure 1, but for the object PKS 2255-282.

of flux, although a γ-ray flare was detected earlier from the object by EGRET in 1997 December (D. J. Macomb et al. 1999). The EGRET outburst lasted from 1997 December 30 until 1998 January 12, with possible weak variability of a short timescale of several days (M. Tornikoski et al. 1999). The total flux above 100 MeV was $(1.6 \pm 0.3) \times 10^{-6}$ photons cm^{-2} s^{-1} with a peak flux of $(4.8 \pm 1.1) \times 10^{-6}$ photons cm^{-2} s^{-1}. This was higher than the quiescent upper limits to emission, based upon previous EGRET observations, by a factor of 20, placing PKS 2255-282 among EGRET's brightest blazars. Before this outburst, PKS 2255-282 had been in the field of view of EGRET several times but was not detected in γ-rays; see Figure 2 in D. J. Macomb et al. (1999). In 1997 November, EGRET recorded a flux above 100 MeV of $(4.7 \pm 2.3) \times 10^{-7}$ photons cm^{-2} s^{-1} (3σ detection), which is about 10 times smaller than the flux from the outburst of 1998 January. The count rate dropped by roughly a factor of 3 by the end of the outburst period (M. Tornikoski et al. 1999). As EGRET was in reduced field mode during the outburst period, the 9.2σ detection only corresponds to 51 ± 9 source counts. With such sparse data, it was difficult to locate γ-ray variability. However, many photons were clustered around two separate times, from 1998 January 2.2 to 3.1 and from 1998 January 9.1 to 10.5. It is noteworthy that a prolonged quiescent state with reported upper limits preceded the outburst observed by EGRET and this was, to some extent, repeatedly observed later on by Fermi-LAT.

For the sake of performing the periodicity search for both objects, PKS 2155-83 and PKS 2255-282, we proceed as follows: We generated LCs with 1 month and 2 months of time binning, encompassing the approximately 15.6 yr (MJD: 54683–60369) of LAT data in the energy range 100 MeV–500 GeV (Figures 1 and 2). A 1 m binned LC with detected bins contingent on test statistics >4 ($TS = 2\log(L/L_0)$, where L and L_0 are the maximum likelihood of the models with and without a source at the target position) was constructed to allow inspection of the flux variation in relatively moderate details. The choice of 2 m binning with $TS > 9$ is motivated by keeping the time intervals long enough to diminish the missing values, reduce fluctuations, and provide better statistics of the underlying variations within the data on the cost of losing the time resolution. The detection ratios (the number of detections in the LC to the total number of bins) in 1 m and 2 m are comparable and estimated to be about 64% and 81% for PKS 2155-83 and PKS 2255-282, respectively. The LCs were then reduced with the maximum likelihood method using Fermitools version 2.2.0[4] by the implementation of the Python package fermipy[5] (Version 1.2.2; M. Wood et al. 2017). The instrument response function P8R3_SOURCE_V3 was used with "SOURCE" class photons.

In this analysis, the photons within the region of interest (ROI; a $15^\circ \times 15^\circ$ square centered on the position of the source of interest) were selected. Photons were then modeled by accounting for the point sources in the 4FGL catalog that positioned around the source of interest (up to 20°). Moreover, the background emission was also modeled with including a galactic component (the Milky Way's diffuse γ-ray emission; *gll_iem_v*07.fits file) and an extragalactic one (the isotropic γ-ray emission from celestial and residual charged-particle backgrounds; *iso_P8R3_SOURCE_V*3_*v*1.txt file). A cut on the zenith angle larger than 90° was imposed to exclude γ-ray augmentation from the Earth limb. Additionally, we used the recommended data quality cuts (DATA QUAL> 0)&&(LAT CONFIG== 1) and removed time periods coinciding with γ-ray bursts and solar flares detected by the LAT. A $0^\circ.1$ spatial binning and eight logarithmic energy bins per decade were adopted. The normalizations of all sources within 3° away from the ROI center and the galactic and isotropic diffuse backgrounds, as well as the normalization and spectral index of the target source, were left free to vary in the likelihood analysis over the full time range of the observation. All other parameters were set at their catalog values. The routines gta.optimize() and gta.fit() were iteratively run until a good fit quality is achieved (fit_quality = 3). To construct the LCs, we split the data for each source into 1 m and 2 m bins and conducted a full likelihood fit in each bin. This is done while utilizing the parameters' values obtained from the full time range analysis. The spectral parameters of the target except the scale parameter were left free during the fit. The normalizations of sources

[4] http://fermi.gsfc.nasa.gov/ssc/data/analysis/software
[5] http://fermipy.readthedocs.io

within 3° from the center of the ROI along with the normalizations of diffuse components, were left to vary.

The observed γ-ray fluxes of both objects display striking variation (Figures 1 and 2). The average flux of the 1 m binned LCs is $F_{\rm av} = (6.12 \pm 4.64) \times 10^{-8}$ photons cm^{-2} s^{-1} and $F_{\rm av} = (1.05 \pm 1.02) \times 10^{-7}$ photons cm^{-2}s^{-1} for PKS 2155-83 and PKS 2255-282, respectively, and that for the 2 m binned LCs is $F_{\rm av} = (6.16 \pm 0.53) \times 10^{-8}$ photons cm^{-2} s^{-1} and $F_{\rm av} = (1.04 \pm 0.90) \times 10^{-7}$ photons cm^{-2} s^{-1} for PKS 2155-83 and PKS 2255-282, respectively.

Photon spectral indices ($\Gamma_{\rm av}$) are estimated to be 2.39 ± 0.39 (1 month) and 2.40 ± 0.29 (2 month) for PKS 2155-83, and 2.41 ± 0.34 (1 month) and 2.45 ± 0.26 (2 month) for PKS 2255-282. Both sources show soft intrinsic γ-ray spectra like most FSRQs (G. G. Madejski & M. Sikora 2016) for both 1 m and 2 m binned LCs. This probably explains the absence of γ-ray detection from these sources at higher energies. PKS 2155-83 (Pearson correlation coefficient $\rho_{1\,\rm m} = 0.28$) and PKS 2255-282 ($\rho_{1\,\rm m} = 0.01$) showed no flux–photon index correlation along the full time range of observation implying that both objects may favor the association with apparent geometrical effects.

2.2. Flux Distribution

An essential feature of an astronomical source's variability is the distribution of the photon flux. The distinction between the two most common Gaussian and lognormal distributions can help characterize the inherent physical process causing the observed variability (Z. Shah et al. 2018; P. J. Morris et al. 2019; F. M. Rieger 2019; Z. Shah et al. 2020). A Gaussian distribution reflects a linear random process, where the flux variation is to be indicated by the distribution width (A. Sinha et al. 2018). In this case, an additive statistical model is implied, with the linear summation of components taking part in building up the emission (e.g., shot noise or a linear summation of many "minijets"). Recent findings, on the other hand, preferentially advocate the lognormal distribution for blazars at various wavelengths and timescales (A. Abramowski et al. 2010; A. Sinha et al. 2017; C. Romoli et al. 2018; Z. Shah et al. 2018; N. Wang et al. 2023).

The lognormality of blazars' fluxes can be linked to the existence of a multiplicative process (F. M. Rieger 2019). Accretion disk fluctuations could be a possible origin for such action, as in the case of X-ray binaries (Y. E. Lyubarskii 1997; P. Arevalo & P. Uttley 2006). In this case, the accretion rate of mass varies as the result of an independent accretion disk's density fluctuations on a timescale that corresponds to the local viscous timescales. The fluctuations proliferate inward and provide a multiplicative process as they couple together in the innermost part of the disk (Y. E. Lyubarskii 1997; A. R. King et al. 2004; P. Arevalo & P. Uttley 2006). If the instabilities in the accretion flow exhibit a quasiperiodic nature, the resulting QPOs will also propagate to the jet, and corresponding emission may be observed (F. M. Rieger & F. Volpe 2010). By analogy, such origins for the lognormality may favor a binary BH scenario for the possible quasiperiodic time signal. Lognormal flux distributions may also originate from cascade-related scenarios, such as magnetospheric inverse-Compton pair production cascades (A. Levinson & F. Rieger 2011) or proton-induced synchrotron cascades (K. Mannheim 1993). Further, the lognormal distribution could also be traced back to the acceleration process itself, for example, with linear Gaussian fluctuations in the particle acceleration rate inside the region of acceleration (A. Sinha et al. 2018). Finally, it should be mentioned that additive processes in specific scenarios can also lead to flux lognormality such as the overall flux (experienced Doppler boosting) from a large number of minijets within a jet with random orientations (J. Biteau & B. Giebels 2012).

For each object, we constructed a flux histogram for the 1 m binned LC chosen over 2 m binned data because it simply provides a statistically more significant fit of the distribution. The probability density function (pdf) of PKS 2155-83 and PKS 2255-282 were fitted by Gaussian $G(\phi)$ and lognormal $L(\phi)$ distributions given by

$$G(\varphi|\mu,\,\sigma) = \frac{1}{\sqrt{2\pi}\,\sigma}\exp\left(-\frac{(\varphi-\mu)^2}{2\sigma^2}\right) \quad (1)$$

and

$$L(\varphi|\mu,\,\sigma) = \frac{1}{\sqrt{2\pi}\,\sigma\varphi}\exp\left(-\frac{(\log_{10}(\varphi)-\mu)^2}{2\sigma^2}\right), \quad (2)$$

where μ and σ are the mean and standard deviation, respectively.

For PKS 2155-83 pdf, the lognormal distribution ($r^2_{1\,\rm m} = 0.94$) seems to be preferred over a Gaussian ($r^2_{1\,\rm m} = 0.88$), which invokes a nonlinear, multiplicative process for the underlying variability rather than additive models. On the contrary, the PKS 2255-282 pdf has a comparable degree of fitness with both distributions; $r^2_{1\,\rm m} = 0.99$ and $= 0.95$ for Gaussian and lognormal distributions, respectively. The Gaussian and lognormal fit parameters, variance, probability, and W-statistic of both sources are listed in Table 1 for 1 m and 2 m cases. The normality test for 1 m and 2 m flux histograms for both objects is rejected.

3. Search for γ-Ray Quasiperiodicity

Several approaches have been used to inspect the quasiperiodic variability in blazars (G. G. Wang et al. 2022). In the present study, different methods were utilized to search for periodicity in the LC. These are described in the following subsections.

3.1. Autocorrelation Function

The autocorrelation function (ACF) is a reliable method suitable for detecting nonsinusoidal periodicities. It involves the correlation of the time series with itself, i.e., with the same series lagged by one or more time units. Constant autocorrelation is associated with a system remaining in the same state from one observation to the next; rapidly decaying ACF indicates a high degree of randomness in the time series, while periodicity in the ACF reflects corresponding periodicity in the data.

The ACF between observations ($f_i(t)$) separated by τ (= 0, 1, 2, 3,..., N) time steps is given by

$$\mathrm{ACF}(\tau) = \frac{\sum_{i=1}^{N-\tau}\{f_i(t) - \hat{f}_{1\to N-\tau}\}\{f_{i+\tau}(t) - \hat{f}_{1+\tau\to N}\}}{(N-\tau)\sigma^2}, \quad (3)$$

where $\hat{f}_{1\to N-\tau}$ and $\hat{f}_{1+\tau\to N}$ are the means of the first (from the first to $N-\tau$ observations), and the last (from $1+\tau$ to N observations) $N-\tau$ of the data points, respectively.

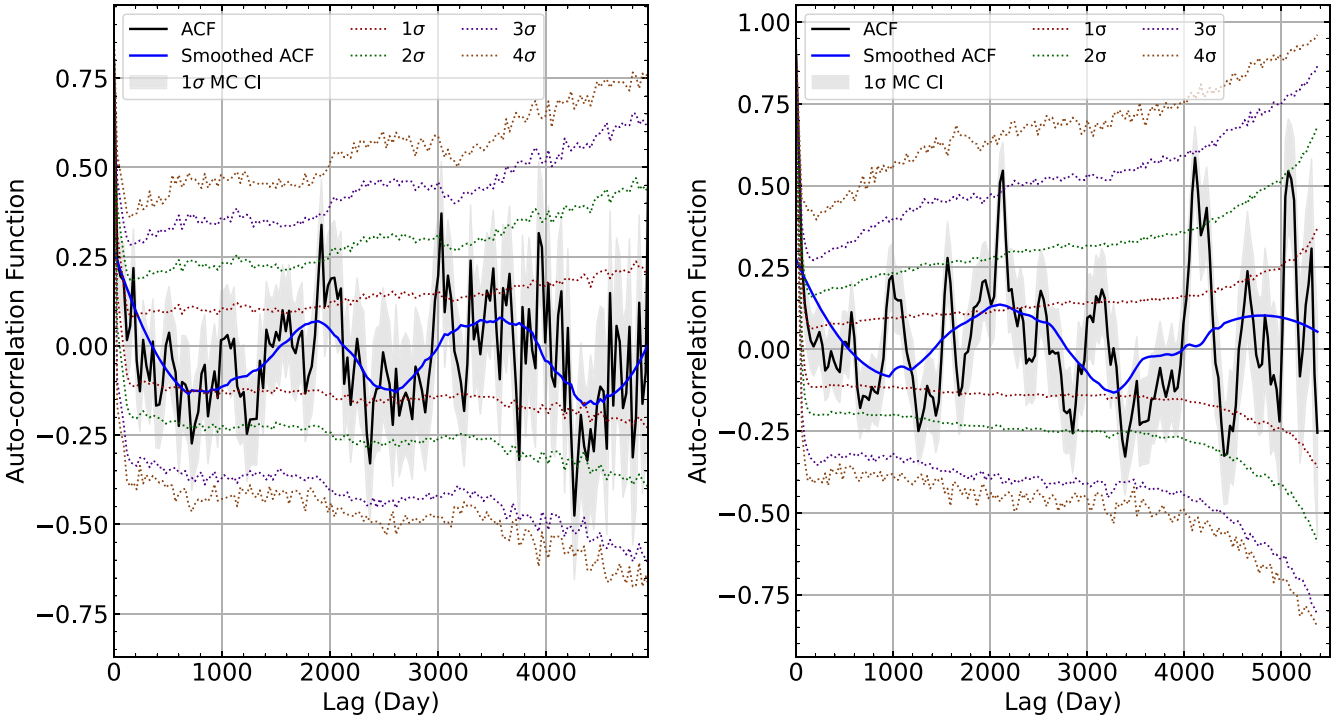

Figure 3. Autocorrelation function for PKS 2155-83 (left panel) and PKS 2255-282 (right panel) 1 m binned LCs. The blue lines represent the smoothed correlation, using a Savitzky–Golay filter. The green, red, indigo, and brown lines represent the local 1σ, 2σ, 3σ, and 4σ chances of observing the autocorrelation levels indicated by the corresponding lines. These were estimated through simulations of 10^5 LCs, utilizing Emmanoulopoulos' method (D. Emmanoulopoulos et al. 2013).

Table 1
Fit Parameters of PKS 2155-83 and PKS 2255-282 pdfs Associated with the Lognormal and Gaussian Distributions, and Flux Normality Tests

Object Name	Binning	Lognormal			Gaussian			Normality Test	
		μ^a	σ^a	r^2	μ^a	σ^a	r^2	$P_{\rm value}$	W-Statistic
PKS 2155-83	1 m	0.49	0.75	0.94	0.39	0.26	0.88	<0.001	0.86
	2 m	0.52	0.69	0.89	0.41	0.21	0.78	<0.001	0.90
PKS 2255-282	1 m	0.80	0.81	0.99	0.28	0.94	0.95	<0.001	0.71
	2 m	0.82	0.76	0.97	0.57	0.68	0.96	<0.001	0.77

Note.
[a] In units of $\times 10^{-7}$ photon cm $^{-2}$ s^{-1}.

We used pyzdcf,[6] a Python module that is utilized for robustly estimating cross-correlation functions of astronomical time-series data that are sparse and unevenly sampled (T. Alexander 1997). A Savitzky–Golay filter[7] was also applied to smooth the ACF, which effectively decreases the low-frequency fluctuations while preserving the overall tendency of the signal (W. H. Press & S. A. Teukolsky 1990). The signal's period is the median of a list of periods computed from the intervals between successive maxima and minima. The uncertainty is determined using the equation proposed by A. McQuillan et al. (2013) as

$$\sigma_P = \frac{1.483 \times \mathrm{MAD}}{\sqrt{N-1}}, \quad (4)$$

where MAD is the periods' median of the absolute deviations implied from the peaks list and N is the number of peaks in the correlation. To determine the significance, we simulated 10^5 LCs, using Emmanoulopoulos' method (D. Emmanoulopoulos et al. 2013) as coded in Python in S. Connolly (2015), that match both the power spectral density and pdf of the object's LC. For each simulated LC, the ACF was applied, and the percentile was computed for each period to estimate the power confidence level.

The obtained ACFs are shown in Figure 3, for 1 m binned LCs. For the 1 m and 2 m binned LCs of PKS 2155-83, the estimated period is at $T = 4.79 \pm 0.35$ yr (2.8σ) and at $T = 4.68 \pm 0.24$ yr (1.8σ), respectively; and for the 1 m and 2 m binned LCs of PKS 2255-282 is at $T = 6.53 \pm 1.34$ yr (3.3σ) and at $T = 6.27 \pm 0.16$ yr (3σ), respectively.

3.2. Date-compensated Discrete Fourier Transform

Another powerful method is the date-compensated discrete Fourier transform (DCDFT), proposed by S. Ferraz-Mello (1981). It tailors to unevenly spaced data, utilizing the notion of function space projection to realize a Fourier transform. For a

[6] https://pypi.org/project/pyzdcf
[7] https://docs.scipy.org/doc/scipy/reference/generated/scipy.signal.savgol_filter.html

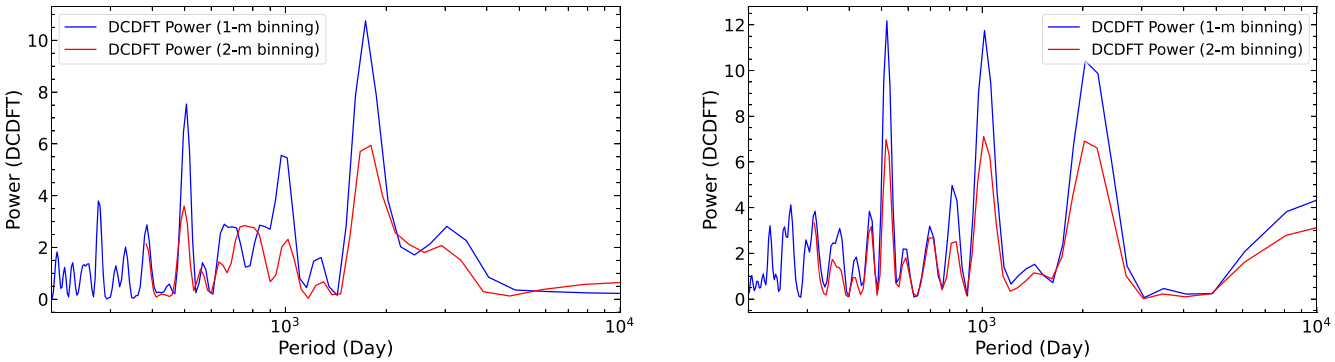

Figure 4. DCDFT of the 1 m (blue line) and 2 m (red line) binned LCs of PKS 2155-83 (left panel) and PKS 2255-282 (right panel).

given test frequency, the power and amplitude of the DCDFT of unequally spaced data are given by

$$P(w, |x\rangle) = \frac{N[\langle y|y\rangle - \langle 1|y\rangle^2]}{2S^2} \quad (5)$$

and

$$A(w, |x\rangle) = \sqrt{2(\langle y|y\rangle - \langle 1|y\rangle^2)}, \quad (6)$$

where N is the number of data points, y is the time simulation function, and S^2 is the variance of the time series. The existence of gaps in the data produces spurious peaks in the power spectrum. The CLEANest algorithm can remove spurious peaks, which can be implemented as explained in G. Foster (1995). We used the AAVSO VStar software[8] (D. Benn 2012) to perform the DCDFT and to run CLEANest period analysis refinement algorithm. In what follows, we enclose the DCDFT values obtained via the DCDFT+CLEANest method by parentheses. The timescales quoted were estimated by fitting the power peak to a Gaussian curve, and uncertainty of the signal is the fitting's half-width at half-maximum (HWHM).

The PKS 2155-83 1 m binned LC showed two clear peaks at 4.84 ± 0.53 yr (4.71 yr) and 1.38 ± 0.05 yr (1.38 yr). Whereas for the 2 m binned LC, it showed only one such peak at 5.00 ± 0.69 yr (4.68 yr), as shown in Figure 4. In the case of PKS 2255-282, the 1 m binned LC showed three peaks at 1.42 ± 0.05 yr (1.42 yr), 2.79 ± 0.17 yr (2.77 yr), and 5.88 ± 0.82 yr (5.64 yr). Comparable results were obtained for the 2 m binned LC.

3.3. The Lomb–Scargle Periodogram

Further method used to search for quasiperiodicity is the Lomb–Scargle periodogram (LSP; N. R. Lomb 1976; J. D. Scargle 1982), which is a widely used algorithm to establish and characterize periodicity in astronomy, even when the LC has gaps and irregularities. The standard normalized LSP is obtained by fitting the LC to sinusoidal waves of the form $y(t) = A\cos(\omega t) + B\sin(\omega t)$. It is defined for a time series (t_i, y_i) as

$$P(\omega) = \frac{1}{2}\left\{\frac{\left(\sum_i y_i \cos\omega(t_i - \tau)\right)^2}{\sum_i \cos^2\omega(t_i - \tau)} + \frac{\left(\sum_i y_i \sin\omega(t_i - \tau)\right)^2}{\sum_i \sin^2\omega(t_i - \tau)}\right\},$$

where τ is specified for each frequency to ensure time-shift invariance, such that

$$\tau = \frac{1}{2\omega}\tan^{-1}\left(\frac{\sum_i \sin(2\omega t_i)}{\sum_i \cos(2\omega t_i)}\right). \quad (7)$$

The generalized Lomb–Scargle periodogram (GLSP) is superior to the standard LSP (M. Ackermann et al. 2015; D. A. Prokhorov & A. Moraghan 2017). Unlike the LSP, the GLSP does not assume that the fitted sine function's mean is the same as the mean of the data. Instead, it accounts for an offset, c, to the fitting sinusoidal function, i.e., $y(t) = A\cos(\omega t) + B\cos(\omega t) + c$. For γ-ray blazars, this term may come from the isotropic diffuse γ-ray background. In addition, the GLSP takes measurement errors into consideration.

The GLSP powers of the 1 m binned LC of PKS 2155-83 is shown in Figure 5. In astronomical observations, spurious peaks can spike up due to various contributing factors (S. Vaughan et al. 2016; J. T. VanderPlas 2018), e.g., window function aliasing and red noise variability background (S. Vaughan 2005). Therefore, the estimated period uncertainty is an essential aspect of reporting the periodogram's results. The false alarm probability (FAP) is one way to quantify peak significance. In the periodograms of PKS 2155-83, the best periods of maximum powers were found to be $T = 4.45 \pm 0.13$ yr with a FAP of 4.51×10^{-11} and $T = 4.42 \pm 0.08$ yr with a FAP of 3.64×10^{-8} for the 1 m and 2 m binned LCs, respectively.

Not only the gaps and observation errors influence the periodogram result, but also the bin size has a remarkable impact, particularly on the high-frequency signal. PKS 2155-83 was reported with a QPO signal at $T = 1.4 \pm 0.1$ yr (2.8σ ; P. Peñil et al. 2020) in agreement with the present result of $T = 1.43 \pm 0.05$ yr (2.5σ) for the 1 m binned LC. This high-frequency signal disappeared in the 2 m binning LC's periodogram, as the variation details decrease.

To further examine the significance of the power peaks, the 10^5 simulated LCs were used. The period was estimated by fitting the power peak to a Gaussian curve, and its uncertainty is the fitting's HWHM. In this way, a peak was identified with a period of 4.69 ± 0.79 yr for the 1 m binned LC and 4.55 ± 0.84 yr for the 2 m binned LC at a significance of (3σ) for both of them (Table 2).

The estimated periods corresponding to the maximum powers in the periodograms of the 1 m and 2 m binned LCs of PKS 2255-282 were $T = 6.16 \pm 0.27$ yr with a FAP of 1.95×10^{-8} and $T = 6.12 \pm 0.41$ yr with a FAP of 8.26×10^{-3}, respectively. The GLSP of the PKS 2255-282 1 m binned

[8] https://www.aavso.org/vstar

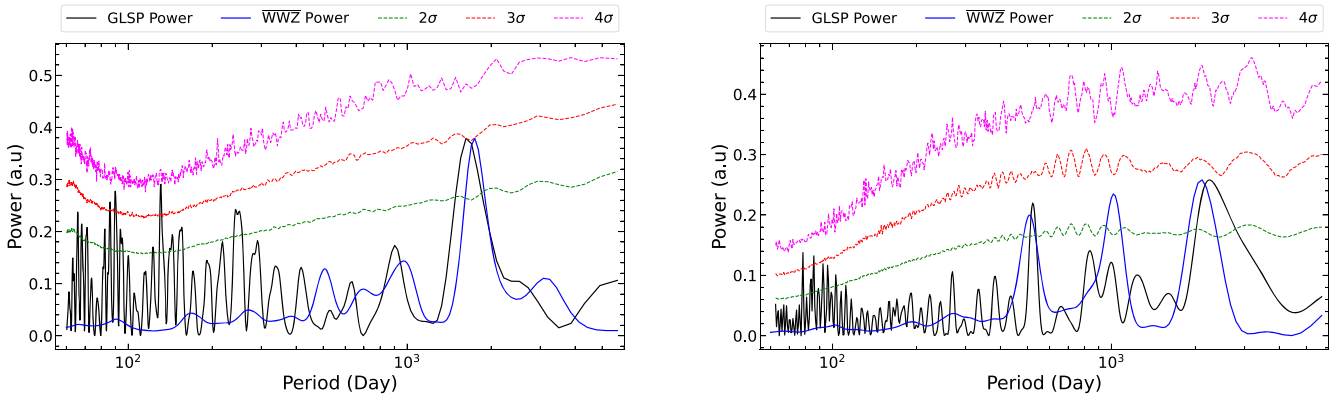

Figure 5. The GLSPs and WWZs of PKS 2155-83 (left panel) and PKS 2255-282 (right panel) γ-ray 1 m binned LCs. The GLSPs are represented in black lines and the WWZs are represented in blue lines. The green, red, and magenta lines represent the 2σ, 3σ, and 4σ confidence levels, respectively, of the GLSPs of 10^5 simulated LCs utilizing Emmanoulopoulos' method (D. Emmanoulopoulos et al. 2013).

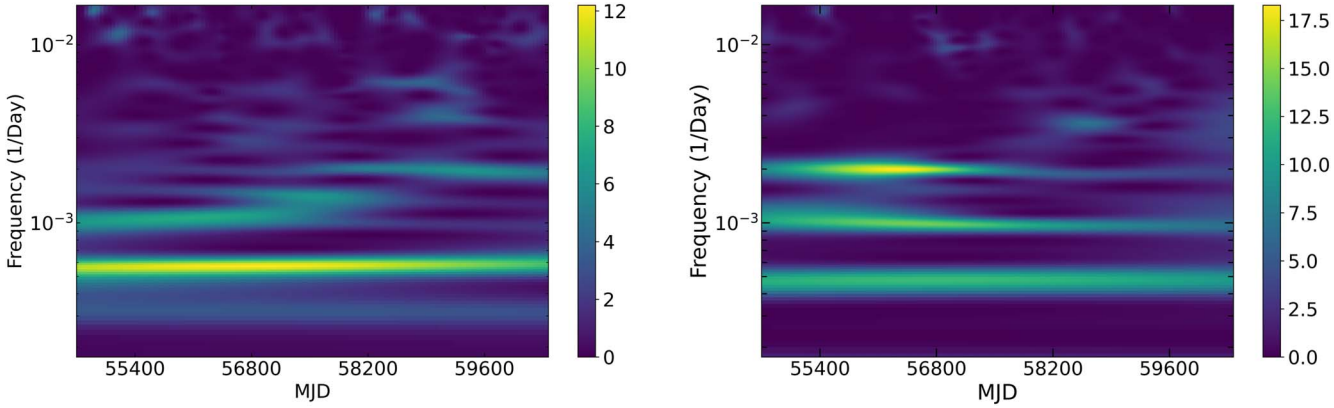

Figure 6. Two-dimensional contour plots of the WWZ power for the 1 m binned LCs of PKS 2155-83 (left panel) and PKS 2255-282 (right panel).

Table 2
The Estimated Periods of the ∼15.6 yr 1 m and 2 m Binned LCs of PKS 2155-83 and PKS 2255-282 with Their Estimated Significance

Object Name	Binning	Power[a] Pn[zk]	Period T[Pn] (yr)	FAP	Chance Prob.	Period T[sim.] (yr)	Signif.
PKS 2155-83	1 m	0.38	4.5 ± 0.13	4.5×10^{-11}	4.8×10^{-13}	4.69 ± 0.79	3σ
	2 m	0.51	4.4 ± 0.08	3.6×10^{-8}	3.3×10^{-10}	4.55 ± 0.84	3σ
PKS 2255-282	1 m	0.26	6.2 ± 0.27	2.0×10^{-8}	2.2×10^{-10}	1.43 ± 0.05–6.82 ± 2.25	2.5σ–2.8σ
	2 m	0.21	6.1 ± 0.41	8.3×10^{-3}	1.8×10^{-4}	6.73 ± 1.35	2.6σ

Note.
[a] The maximum power using the Zechmeister and Kuerster normalization.

LC showed periods (in years) of 1.43 ± 0.05 (2.5σ) and 6.82 ± 2.25 (2.8σ) (as shown in Figure 5), while the GLSP of the 2 m binned LC showed only the low-frequency period at $T = 6.73 \pm 1.35$ yr with a significance of 2.6σ (Table 2).

3.4. The Weighted Wavelet Z-transform

An additional efficient method for detecting periodicity associated with LCs of uneven data sampling is the weighted wavelet z-transform (WWZ; G. Foster 1996). It is based on a similar notion as the LSP, where the data are fitted by sinusoidal waves. The WWZ can record the possible existence of quasiperiodic variability with a transient nature, where the waves are localized in both frequency and time domains (P. Mohan & A. Mangalam 2015; G. Bhatta et al. 2016; F. A. Benkhali et al. 2020).

For the PKS 2155-83 LC, the WWZ gave (see Figures 5 and 6) a peak at a period of 4.88 ± 0.61 yr and 4.93 ± 0.74 yr for the 1 m and 2 m binned LCs, respectively. The WWZ of PKS 2255-282 gave a period of 5.87 ± 0.85 yr and 5.81 ± 0.85 yr for the 1 m and 2 m binned LCs, respectively. In addition, the WWZ of the PKS 2255-282 1 m binned LC displays a notable peak at a period of about 1000 days.

3.5. REDFIT

The LSP and WWZ are strongly affected by red noise at low frequencies, where they place peaks that mimic a real periodicity. The REDFIT method is a suitable tool for detecting

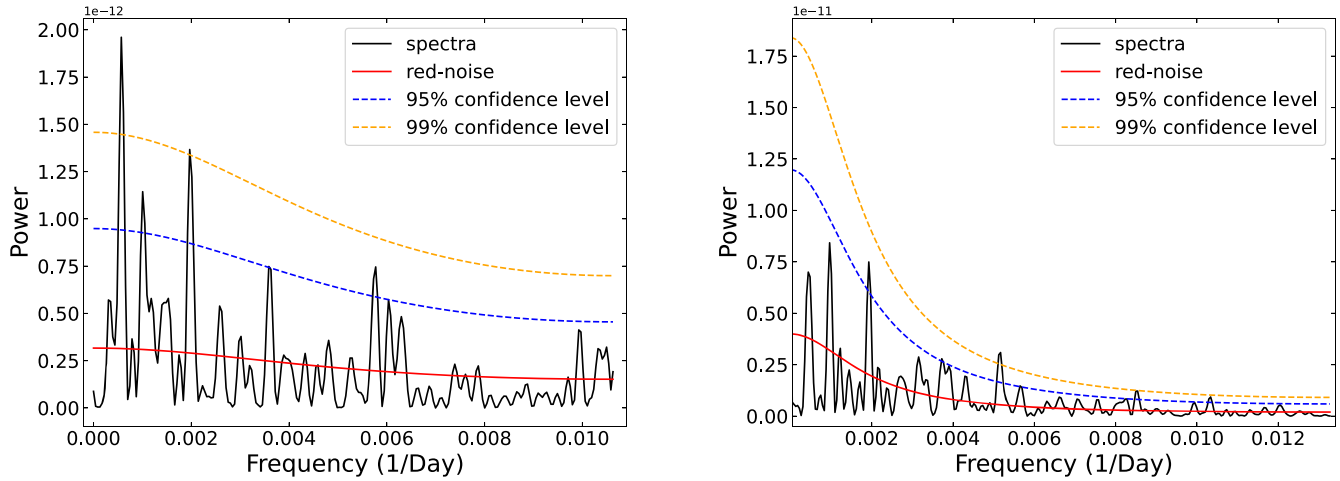

Figure 7. REDFIT periodicity analysis for the 1 m binned LCs of PKS 2155-83 (left panel) and PKS 2255-282 (right right). The bias-corrected power spectrum is represented by the black line. Spectrum of the theoretical red noise (red line), 95% confidence level (blue dashed line), and 99% confidence level (orange dashed line) were estimated by fitting the data with the AR1 process.

periodicity in the dominant red noise LCs of blazars. It simply uses a first-order autoregressive (AR1) model (K. Hasselmann 1976) to precisely assess the periodogram peaks against stochastic fluctuations (H. Zhang et al. 2021). The method was coded in Fortran 90 by M. Schulz & M. Mudelsee (2002). We used the REDFIT3.8e3 package in the present analysis.[9]

Compatible with previous estimates, the results for PKS 2155-83 suggest a period of 4.82 ± 0.55 yr at significance exceeding 99% and 4.63 ± 0.62 yr at 2.2σ (Figure 7) for the 1 m and 2 m binned LCs, respectively. The results furthermore suggest another peak of $T = 1.37$ yr at 2.5σ and 2σ for the 1 m and 2 m binned LCs, respectively. For the 1 m and 2 m binned LCs of PKS 2255-282, no significant signal was detected except for a period of about 550 days, as previously reported (P. Peñil et al. 2020), at significance of 2.3σ and 2.4σ for the 1 m and 2 m binned LCs, respectively. It should be noted that the maximum significance provided by REDFIT is limited to 2.5σ.

4. Summary and Discussion

The growing number of reports regarding the possible existence of quasiperiodicities in the light curves of blazars is interesting; in terms of the information it may embody on the emission processes of these systems, as well as the possibility of detecting binary SMBH systems in the process of merging. A larger sample of candidate objects should include going beyond the well-sampled light curve, where the majority of its time bins have significant observations and only a minority constitute observations with upper limits or gaps.

Here, we studied two such cases of FSRQs from the Fermi-LAT fourth catalog. The 1 m and 2 m binned γ-ray LCs were then generated via the maximum likelihood technique in the energy range 100 MeV–500 GeV for about 15.6 yr. The selected time bins provided data points with a signal-to-noise ratio above 2σ for a bin size of 1 month and 3σ for a bin size of 2 months. The LCs of the two sources showed distinctive behaviors of high- and low-state alternation. PKS 2155-83 displayed four high states in 2010, 2014, 2019, and 2023, interspersing its otherwise low state. PKS 2255-282 showed three high states in 2009–2013, 2017–2021, and 2023 up to the end of data interrupting its low state.

The pdf of PKS 2155-83 tended toward lognormality, especially in the case of the 1 m binned LC, indicative of a nonlinear, multiplicative processes underlying the variability, rather than an additive stochastic process (e.g., associated with many superposed "minijets" in an AGN engine or simple shot noise). The pdf of PKS 2255-282, on the other hand, revealed a comparable degree of fitness with both lognormal and Gaussian distributions.

Various methods were applied to the LCs to assess the possible existence of quasiperiodicity. Namely, the ACF, the date-compensated discrete Fourier transform, the GLSP, the WWZ, and the REDFIT algorithm. Periodicity peaks were found, using these methods, for PKS 2155-83 in the ranges (in years) 4.45 ± 0.13–5.03 ± 0.68 and 4.42 ± 0.08–4.93 ± 0.74 for 1 m and 2 m binned LCs, respectively. While, for PKS 2255-282, they were found in the ranges of 5.87 ± 0.85–6.82 ± 2.25 and 5.81 ± 0.85–6.73 ± 1.35 for 1 m and 2 m binned LCs, respectively. For example, the GLSP of PKS 2155-83 showed periods at 4.69 ± 0.79 yr and at 4.55 ± 0.84 yr for the 1 m and 2 m binned LCs, respectively. Both with significance 3σ. The PKS 2255-282 1 m binned LC showed two possible periods at 1.43 ± 0.05 yr (2.5σ) and 6.82 ± 2.25 yr (2.8σ), while the 2 m binned LC showed a period at 6.73 ± 1.35 yr (2.6σ) and no noticeable high-frequency signal. Recently, results of 19 blazars were reported using the first 12 yr of data from the Fermi-LAT and multiwavelength archival data from radio, infrared, and optical bands (P. Peñil et al. 2024). This study reported no periodic modulations from PKS 2255-282 except of 1.4 ± 0.1 yr (2–3σ) from the cross correlation between γ-rays and the V band. The disagreement between the suggested periodicity in the present work and the results from the optical observation may argue for the difference between the optical emission region and/or mechanism and the corresponding ones for gamma radiation.

The existence and origins of QPOs in blazars are still controversial (E. Sobacchi et al. 2017; A. Sandrinelli et al. 2018; M. Tavani et al. 2018). If confirmed, periodicities may be linked to the process feeding the jet and/or to the relativistic jet itself (M. Ackermann et al. 2015). They may in general involve scenarios invoking a binary SMBH AGN system (as, for

[9] https://www.marum.de/Prof.-Dr.-michael-schulz/Michael-Schulz-Software.html

example, discussed in J. Zhou et al. 2018). Intrinsic origins include possible oscillations associated with instability in the accretion disk or jet formation region (A. Tchekhovskoy et al. 2011). The characteristic timescales of the pulsational accretion flow instabilities can range from minutes to hours (F. Honma et al. 1992; A. Tchekhovskoy & J. C. McKinney 2012). This is outside the periods suggested in this study. Nonetheless, in the case of slow-spinning SMBHs, magnetohydrodynamics simulations of magnetically choked accretion flow produce longer frequencies (A. Tchekhovskoy & J. C. McKinney 2012).

Another possible origin of QPOs in blazars could also be associated with apparent geometrical effects (F. M. Rieger 2004), e.g., jet precession/helical jet (N. Vlahakis & K. Tsinganos 1998; P. E. Hardee & A. Rosen 1999; M. Villata & C. Raiteri 1999; L. Ostorero et al. 2004; M. Nakamura & D. L. Meier 2004; A. Caproni et al. 2013; E. Sobacchi et al. 2017). In such cases, the observed flux will undergo periodic modulation due to the periodic variation of the Doppler magnification factor (M. Ackermann et al. 2015). This scenario does not need intrinsic flux modulation and does not induce oscillations in the spectral index. PKS 2155-83 and PKS 2255-282 showed no flux–photon index correlation along the full time range of observation (∼15.6 yr; with time binning of 1 month and 2 months). Therefore, both objects may favor this second origin.

Merging SMBHs (M. C. Begelman et al. 1980; J. E. Barnes & L. Hernquist 1992) may induce both types of (intrinsic and geometrical) quasiperiodicities. In particular, an SMBH binary system with a milliparsec separation and a total mass of $\sim 10^8 M_\odot$ in the early inspiral gravitational-wave driven regime would induce jet precession with timescales of SMBH binary-induced periodicities are ranging from ∼1 to ∼25 yr (F. M. Rieger 2007; S. Komossa & J. A. Zensus 2016; E. Sobacchi et al. 2017). Given the redshifts of PKS 2155-83 ($z = 1.865$) and PKS 2255-282 ($z = 0.926$), reflecting cosmological epochs when merging between galaxies and their embedded BHs were still relatively frequent, the binary BH scenario may be, in principle, especially relevant.

We considered a simple model within this general framework (E. Sobacchi et al. 2017). It assumes a binary system of SMBHs on circular orbits. The direction of the jet, carried by one SMBH, in the center of mass frame is perpendicular to the orbital plane. The jet deviates with an angle $\Delta\alpha$, due to the imprint of the orbital velocity, v, of the jet-carrying BH on the highly relativistic jet. Consequently, the angle $\theta_{\rm obs}$ between the jet and the distant observer oscillates with an amplitude $\Delta\theta_{\rm obs}$, with the same period T of the orbital motion.[10] This simple model thus incorporates features (in particular, a characteristic timescale) that may be generic to potential blazar quasiperiodic signals originating from binary SMBH systems.

Based on this model and the periodicities suggested by the GLSP, where $T_{\rm int}$ is 1.64 and 3.63 yr, for PKS 2155-83 and PKS 2255-282, respectively, one can estimate the total BH masses. In this context, the total masses (as a function of $\Delta\theta_{\rm obs}$ and mass ratio q) are

$$M = 1.4 \times 10^8 \left(\frac{1+q}{q}\right)^3 \left(\frac{\Delta\theta_{\rm obs}}{5^\circ}\right)^3 M_\odot \quad (8)$$

and

$$M = 3.0 \times 10^8 \left(\frac{1+q}{q}\right)^3 \left(\frac{\Delta\theta_{\rm obs}}{5^\circ}\right)^3 M_\odot \quad (9)$$

for PKS 2155-83 and PKS 2255-282, respectively. The separation of the binary is found to be, with $\Delta\theta_{\rm obs} = 5^\circ$, $R = 0.0035(1+q)/q$ pc and the SMBH merging timescale is $T_{\rm GW} = 3.2 \times 10^4 q(q/(1+q))^3$ yr for PKS 2155-83. A similar exercise gives a separation of the binary $R = 0.0104(1+q)/q$ pc and the SMBH merging timescale is $T_{\rm GW} = 6.9 \times 10^4 q(q/(1+q))^3$ yr for PKS 2255-282. Note that the jet has to be assumed to be carried by the secondary SMBH (i.e., $q \gtrsim 1$) to avoid extremely short timescales of orbital decay.

Although the results are quite sensitive to $\Delta\theta_{\rm obs}$, the deflection angle of the highly relativistic jet $\Delta\alpha$, and therefore the amplitude $\Delta\theta_{\rm obs}$, are constrained to a small angle, where $\Delta\alpha \simeq v/c = (q/(1+q))(GM/Rc^2)^{1/2}$ and $\Delta\theta_{\rm obs} = 2\Delta\alpha$. In order to have observable consequences on the QPO timescales inferred one needs this angle to be of the order of a few degrees (E. Sobacchi et al. 2017).

The inferred combined BH masses are comparable, with reasonable estimation, in both cases considered with independent estimates of the compact central masses estimated in the respective galaxies (e.g., via dynamical virial equilibrium calculations reported in literature, D. R. Xiong & X. Zhang 2014, where it is found that $\log_{10}(M_{\rm BH}/M_\odot)$ were 9.02 and 9.16 for PKS 2155-83, M. S. Shaw et al. 2012, and 8.92 and 9.16 for PKS 2255-282, M. Gu et al. 2001). Such SMBHs are inferred to be abundant at much higher redshifts. Further searches for high-redshift blazars with potential periodicities, in conjunction with gravitational-wave signals from SMBH systems from future detectors, such as LISA, may thus serve to test the consistency of the merging BH scenario as an origin of such signals. This may, in turn, potentially shed light on the SMBH merger rate in the context of standard hierarchical galaxy formation in standard cosmology, ultimately providing a test of the model itself.

[10] Note that the intrinsic period $T_{\rm int}$ is shorter than the observed period $T_{\rm obs}$ by a factor of $1/(1+z)$.

Acknowledgments

We thank the referee for a careful reading and insightful suggestions that helped improve our manuscript. We also acknowledge the use of Fermitools-conda, DELCgen-Simulating light curves (S. Connolly 2015), Matplotlib (J. D. Hunter 2007), Savgol filter (P. Virtanen et al. 2020), pyZDCF, PyAstronomy (S. Czesla et al. 2019), NumPy (C. R. Harris et al. 2020), AAVSO VStar software (D. Benn 2012), REDFIT (M. Schulz & M. Mudelsee 2002), astroML (Ž. Ivezić et al. 2014).

References

Abdollahi, S., Acero, F., Baldini, L., et al. 2022, ApJS, 260, 53
Abhir, J., Joseph, J., Patel, S. R., & Bose, D. 2021, MNRAS, 501, 2504
Abramowski, A., Acero, F., Aharonian, F., et al. 2010, A&A, 520, A83
Ackermann, M., Ajello, M., Albert, A., et al. 2015, ApJL, 813, L41
Alexander, T. 1997, Astronomical Time Series, Vol. 218 (Dordrecht: Springer), 163
Arevalo, P., & Uttley, P. 2006, MNRAS, 367, 801
Atwood, W. B., Abdo, A. A., Ackermann, M., et al. 2009, ApJ, 697, 1071
Barnes, J. E., & Hernquist, L. 1992, ARA&A, 30, 705
Begelman, M. C., Blandford, R. D., & Rees, M. J. 1980, Natur, 287, 307
Benkhali, F. A., Hofmann, W., Rieger, F., & Chakraborty, N. 2020, A&A, 634, A120
Benn, D. 2012, JAAVSO, 40, 852
Bhatta, G., & Dhital, N. 2020, ApJ, 891, 120

Bhatta, G., Zola, S., Stawarz, Ł., et al. 2016, ApJ, 832, 47
Biteau, J., & Giebels, B. 2012, A&A, 548, A123
Blandford, R., Meier, D., & Readhead, A. 2019, ARA&A, 57, 467
Błazejowski, M., Blaylock, G., Bond, I. H., et al. 2005, ApJ, 630, 130
Caproni, A., Abraham, Z., & Monteiro, H. 2013, MNRAS, 428, 280
Caproni, A., Abraham, Z., Motter, J. C., & Monteiro, H. 2017, ApJL, 851, L39
Charlot, P., Boboltz, D. A., Fey, A. L., et al. 2010, AJ, 139, 1713
Connolly, S. 2015, arXiv:1503.06676
Czesla, S., Schröter, S., Schneider, C. P., et al., 2019 PyA: Python astronomy-related packages, Astrophysics Source Code Library, ascl:1906.010
Dutka, M., DAmmando, F., & Ojha, R. 2012, ATel, 3948, 1
Emmanoulopoulos, D., McHardy, I. M., & Papadakis, I. E. 2013, MNRAS, 433, 907
Fabricius, C., Luri, X., Arenou, F., et al. 2021, A&A, 649, A5
Ferraz-Mello, S. 1981, AJ, 86, 619
Foster, G. 1995, AJ, 109, 1889
Foster, G. 1996, AJ, 112, 1709
Gu, M., Cao, X., & Jiang, D. R. 2001, MNRAS, 327, 1111
Hardee, P. E., & Rosen, A. 1999, ApJ, 524, 650
Harris, C. R., Millman, K. J., Van Der Walt, S. J., et al. 2020, Natur, 585, 357
Hashad, M., EL-Zant, A. A., & Abdou, Y. 2023, AdSpR, 72, 3538
Hasselmann, K. 1976, Tell, 28, 473
Honma, F., Matsumoto, R., & Kato, S. 1992, PASJ, 44, 529
Hunter, J. D. 2007, CSE, 9, 90
Ivezić, Ž., Connolly, A. J., VanderPlas, J. T., & Gray, A. 2014, Statistics, Data Mining, and Machine Learning in Astronomy (Princeton, NJ: Princeton Univ. Press)
Jones, D. H., Read, M. A., Saunders, W., et al. 2009, MNRAS, 399, 683
King, A. R., Pringle, J. E., West, R. G., & Livio, M. 2004, MNRAS, 348, 111
Komossa, S., Baker, J. G., & Liu, F. K. 2016, in IAU Symp. 29B, Astronomy in Focus (Cambridge: Cambridge Univ. Press), 292
Komossa, S., & Zensus, J. A. 2016, in IAU Symp. 312, Star Clusters and Black Holes in Galaxies across Cosmic Time (Cambridge: Cambridge Univ. Press), 13
Levinson, A., & Rieger, F. 2011, ApJ, 730, 123
Liao, N. H., Bai, J. M., Liu, H. T., et al. 2014, ApJ, 783, 83
Lister, M. L., Aller, H. D., Aller, M. F., et al. 2009, AJ, 137, 3718
Lomb, N. R. 1976, Ap&SS, 39, 447
Lyubarskii, Y. E. 1997, MNRAS, 292, 679
Macomb, D. J., Gehrels, N., & Shrader, C. R. 1999, ApJ, 513, 652
Madau, P., & Dickinson, M. 2014, ARA&A, 52, 415
Madejski, G. G., & Sikora, M. 2016, ARA&A, 54, 725
Mannheim, K. 1993, A&A, 269, 67
Mauch, T., Murphy, T., Buttery, H. J., et al. 2003, MNRAS, 342, 1117
McQuillan, A., Aigrain, S., & Mazeh, T. 2013, MNRAS, 432, 1203
Mezcua, M., Pacucci, F., Suh, H., Siudek, M., & Natarajan, P. 2024, ApJL, 966, L30
Mohan, P., & Mangalam, A. 2015, ApJ, 805, 91
Morris, P. J., Chakraborty, N., & Cotter, G. 2019, MNRAS, 489, 2117
Nakamura, M., & Meier, D. L. 2004, ApJ, 617, 123
Ostorero, L., Villata, M., & Raiteri, C. 2004, A&A, 419, 913
Peñil, P., Ajello, M., Buson, S., et al. 2022, arXiv:2211.01894
Peñil, P., Domínguez, A., Buson, S., et al. 2020, ApJ, 896, 134
Peñil, P., Otero-Santos, J., Ajello, M., et al. 2024, MNRAS, 529, 1365
Press, W. H., & Teukolsky, S. A. 1990, ComPh, 4, 669
Prokhorov, D. A., & Moraghan, A. 2017, MNRAS, 471, 3036
Ren, H. X., Cerruti, M., & Sahakyan, N. 2023, A&A, 672, A86
Rieger, F. M. 2004, ApJL, 615, L5
Rieger, F. M. 2007, Ap&SS, 309, 271
Rieger, F. M. 2019, Galax, 7, 28
Rieger, F. M., & Volpe, F. 2010, A&A, 520, A23
Romoli, C., Chakraborty, N., Dorner, D., Taylor, A., & Blank, M. 2018, Galax, 6, 135
Sandrinelli, A., Covino, S., Treves, A., et al. 2018, A&A, 615, A118
Scargle, J. D. 1982, ApJ, 263, 835
Schulz, M., & Mudelsee, M. 2002, CG, 28, 421
Shah, Z., Mankuzhiyil, N., Sinha, A., et al. 2018, RAA, 18, 141
Shah, Z., Misra, R., & Sinha, A. 2020, MNRAS, 496, 3348
Shaw, M. S., Romani, R. W., Cotter, G., et al. 2012, ApJ, 748, 49
Sinha, A., Khatoon, R., Misra, R., et al. 2018, MNRAS, 480, L116
Sinha, A., Sahayanathan, S., Acharya, B. S., et al. 2017, ApJ, 836, 83
Sobacchi, E., Sormani, M. C., & Stamerra, A. 2017, MNRAS, 465, 161
Tavani, M., Cavaliere, A., Munar-Adrover, P., & Argan, A. 2018, ApJ, 854, 11
Tchekhovskoy, A., & McKinney, J. C. 2012, MNRAS, 423, L55
Tchekhovskoy, A., Narayan, R., & McKinney, J. C. 2011, MNRAS, 418, L79
Tornikoski, M., Tingay, S. J., Mücke, A., et al. 1999, AJ, 118, 1161
Urry, C. M., & Padovani, P. 1995, PASP, 107, 803
VanderPlas, J. T. 2018, ApJS, 236, 16
Vaughan, S. 2005, A&A, 431, 391
Vaughan, S., Uttley, P., Markowitz, A. G., et al. 2016, MNRAS, 461, 3145
Villata, M., & Raiteri, C. 1999, A&A, 347, 30
Virtanen, P., Gommers, R., Oliphant, T. E., et al. 2020, NatMe, 17, 261
Vlahakis, N., & Tsinganos, K. 1998, MNRAS, 298, 777
Volonteri, M., Bogdanović, T., Dotti, M., & Colpi, M. 2016, in IAU Symp. 29B, Astronomy in Focus (Cambridge: Cambridge Univ. Press), 285
Wallace, E. 2010, ATel, 2373, 1
Wang, G. G., Cai, J. T., & Fan, J. H. 2022, ApJ, 929, 130
Wang, N., Yi, T.-F., Wang, L., et al. 2023, RAA, 23, 115011
Wood, M., Caputo, R., Charles, E., et al. 2017, ICRC (Busan), 301, 824
Xiong, D. R., & Zhang, X. 2014, MNRAS, 441, 3375
Yan, D., Zhou, J., Zhang, P., Zhu, Q., & Wang, J. 2018, ApJ, 867, 53
Yang, Y., Bartos, I., Haiman, Z., et al. 2020, ApJ, 896, 138
Zhang, H., Yan, D., Zhang, P., Yang, S., & Zhang, L. 2021, ApJ, 919, 58
Zhang, P.-f., Yan, D.-h., Zhou, J.-n., Wang, J.-c., & Zhang, L. 2020, ApJ, 891, 163
Zhou, J., Wang, Z., Chen, L., et al. 2018, NatCo, 9, 1